

## Fluorescence Competition Assay Measurements of Free Energy Changes for RNA Pseudoknots<sup>†</sup>

Biao Liu,<sup>‡</sup> Neelaabh Shankar,<sup>§</sup> and Douglas H. Turner<sup>\*‡</sup>

<sup>‡</sup>Department of Chemistry, University of Rochester, Rochester, New York 14627, <sup>§</sup>Department of Biochemistry and Biophysics, School of Medicine and Dentistry, University of Rochester, Rochester, New York 14642

Received September 3, 2009; Revised Manuscript Received November 17, 2009

**ABSTRACT:** RNA pseudoknots have important functions, and thermodynamic stability is a key to predicting pseudoknots in RNA sequences and to understanding their functions. Traditional methods, such as UV melting and differential scanning calorimetry, for measuring RNA thermodynamics are restricted to temperature ranges around the melting temperature for a pseudoknot. Here, we report RNA pseudoknot free energy changes at 37 °C measured by fluorescence competition assays. Sequence-dependent studies for the loop 1–stem 2 region reveal (1) the individual nearest-neighbor hydrogen bonding (INN-HB) model provides a reasonable estimate for the free energy change when a Watson–Crick base pair in stem 2 is changed, (2) the loop entropy can be estimated by a statistical polymer model, although some penalty for certain loop sequences is necessary, and (3) tertiary interactions can significantly stabilize pseudoknots and extending the length of stem 2 may alter tertiary interactions such that the INN-HB model does not predict the net effect of adding a base pair. The results can inform writing of algorithms for predicting and/or designing RNA secondary structures.

RNA pseudoknots are important motifs that are formed by base pairing between the nucleotides in a loop region and complementary bases outside the loop (Figure 1A). They exist widely in viral RNA (1–3), rRNA (4, 5), mRNA (6–10), tmRNA (11, 12), ribozymes (13, 14), telomerase RNA (15–18), aptamers (19), and others and are important for ribosomal frameshifting (20, 21), riboswitches (22), catalysis (13, 17), etc. (23). A typical H-type RNA pseudoknot (Figure 1B) is formed by two stems and two or three loops (2). Loop 1 spans the deep major groove of stem 2, and loop 3 spans the shallow minor groove of stem 1. Loop 2, which is usually zero or one nucleotide, separates stems 1 and 2. For the formation of a pseudoknot, the lengths of the other loops have to meet some requirements (24). Examination of the natural pseudoknots collected in Pseudo-Base (25) revealed different length distributions for each pseudoknot loop and stem (26).

The thermodynamic stability of RNA pseudoknots is a key factor determining structure–function relationships. For example, the stability of a pseudoknot is a major factor determining the efficiency of −1 frameshifting in retroviruses (27, 28). In human telomerase, the pseudoknot domain may act as a molecular switch, in which the pseudoknot and the corresponding hairpin have nearly equal stability in solution (18). Mutations affecting this equilibrium can cause inherited Dyskeratosis congenita (29, 30). In H5N1 influenza A virus, the equilibrium between the pseudoknot and the corresponding hairpin may change virus infectivity (31).

The thermodynamic properties of pseudoknots are also important for predicting RNA structure. Dynamic programming (32, 33) and heuristic (34) algorithms, stochastic simulations (35–37), and an NMR constrained algorithm (38) for predicting RNA

structure including pseudoknots are available. Most such computational approaches use a nearest-neighbor model (39, 40) for predicting the stabilities of stems 1 and 2. This is coupled with various models for the free energy contribution from the loops (26, 41, 42). In these models, the contributions from tertiary interactions between loops and stems are neglected. The models have been benchmarked against a limited set of measured thermodynamics for pseudoknots (24, 43–49). Thus, this paper reports measurements of pseudoknot thermodynamic parameters that can be compared with theoretical predictions. The results should improve identification of pseudoknots and facilitate studies of their importance for function (2).

UV melting (39, 40) and differential scanning calorimetry (DSC) (44, 50) are common methods for measuring RNA thermodynamics. For the unimolecular transitions of a pseudoknot, however, both rely on data acquired near the melting temperatures and on deconvoluting overlapping transitions. Here, we use two versions of fluorescence competition assays (FCA) (51–53) to measure the free energies at 37 °C for a series of pseudoknots derived from the beet western yellow virus (BWYV) H-type pseudoknot (Figure 1), which is important for frameshifting (54). One method uses fluorescence resonance energy transfer (FRET) which has been previously used to determine the free energy of nucleic acid duplexes, in which a fluorescence donor and acceptor are linked to the oligonucleotides (53). The second method uses quenching directly by the RNA rather than by an added acceptor. The results are compared to previous thermodynamic measurements (44, 45), to predictions using various computational models, and to expectations from the crystal structure [Protein Data Bank (PDB) entry 437D (55)]. To test computational pseudoknot free energy models, which neglect tertiary interactions, mutations address the loop 1–stem 2 region which has no tertiary interactions beyond the joint of stems 1 and 2 (Figure 1B).

<sup>†</sup>This work was supported by National Institutes of Health Grant GM22939 (D.H.T.).

<sup>\*</sup>To whom correspondence should be addressed. Phone: (585) 275-3207. Fax: (585) 276-0205. E-mail: turner@chem.rochester.edu.

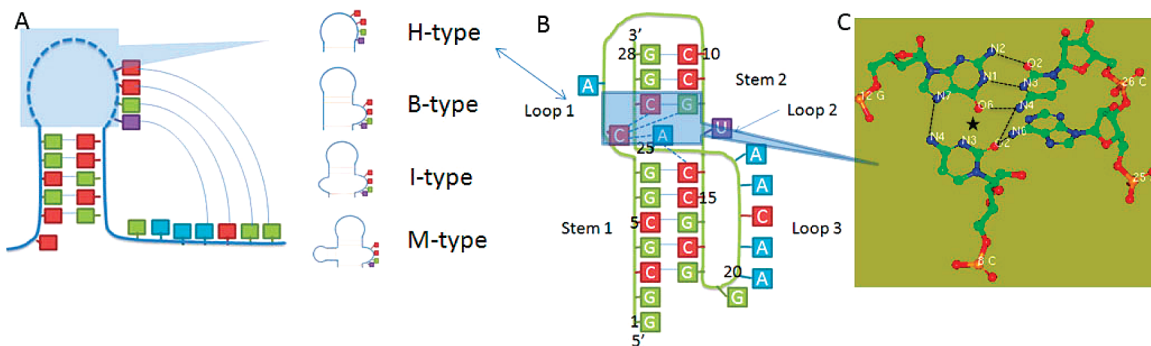


**FIGURE 1:** (A) Pseudoknot formed by base pairing (shown by curved lines) between a loop region (darkened area) and complementary bases outside the loop. The loop region can be a hairpin, bulge, internal, or multibranch loop, corresponding to an H-type, B-type, I-type, or M-type pseudoknot, respectively. (B) Secondary structure of the H-type pseudoknot from BWYV (Protein Data Bank entry 437D), called 437D PSK. Some tertiary interactions between bases in loop 1 and stem 2 in darkened area are shown by dashed lines. Tertiary interactions between loop 3 and stem 1 found in the crystal structure (55) are not shown. (C) Crystal structure of the darkened area. Dashed lines indicate hydrogen bond interactions; there is likely protonation of C8 and therefore an additional hydrogen bond between C8 and G12 as indicated by the star (55).

## MATERIALS AND METHODS

**Materials.** Oligonucleotides were purchased from Integrated DNA Technologies, Inc. (IDT), which purified them by HPLC and tested molecular weights by mass spectroscopy. Fluorescent oligonucleotides had fluorescein attached by a linker of six carbons (6-FAM). The concentrations of single-strand oligonucleotides were calculated from 80 °C absorbance and single-strand extinction coefficients, approximated by IDT by a nearest-neighbor model (56, 57).

**UV Melting of Duplexes.** Optical melting was performed in standard melting buffer [1.0 M NaCl, 20 mM sodium cacodylate, and 0.5 mM Na<sub>2</sub>EDTA (pH 7.0)]. Single strands for forming non-self-complementary duplexes were mixed in 1:1 molar ratios, then annealed at 85 °C for 2 min, and cooled to 5 °C at a rate of ~5 °C/min. Absorbance versus temperature melting curves were measured at 280 nm with a heating rate of 1 °C/min on a Beckman Coulter DU 640 spectrophotometer controlled by a Beckman Coulter high-performance temperature controller cooled with water flow. Duplexes were melted over a 60-fold range in oligonucleotide concentration. Data were analyzed by fitting the transition to a two-state model with sloping baselines using a nonlinear least-squares program (58, 59).

**Fluorescence Competition Assay with a Donor–Acceptor Pair (FCA/DA).** FRET-based titration assays have been used to directly detect free energy differences between a “reference” structure and a related “test” structure of DNA, which allows calculation of the free energy for the test structure (53). Figure 2A illustrates the application of this method for measuring the free energy of an RNA pseudoknot. The pseudoknot (P) is labeled with fluorescein at the 3' end and acts as the FRET donor strand. The fluorescence intensity for the pseudoknot at 10 nM in 250 μL of standard melting buffer is measured and used as the starting point of the titration. In comparison to the BWYV pseudoknot reported elsewhere (44, 45), which is named 437D PSK (Figure 1B), there is a GC dangling 3' end here (Figure 2A), so the fluorescein is not directly adjacent to the pseudoknot. This construct is called PSK 1. The free energy contribution for this dangling 3' end was measured by melting the model duplexes 5'CUGGC/3'FCGGACCG and 5'CUGGC/3'GACCG, where F is fluorescein. To measure the free energy change for the formation of PSK 1, a strand was designed to be Watson–Crick complementary to the sequence at the 3' end of the pseudoknot so that its binding could compete with formation of stem 2 and thus unfold the pseudoknot. This strand was labeled with a quencher (Iowa Black FQ) to serve as an acceptor and named competitor 1. Titrations were performed in 1.0 M

NaCl, 20 mM sodium cacodylate, and 0.5 mM Na<sub>2</sub>EDTA, at pH 6.0, 7.0, or 8.0. Aliquots of a mixture of the concentrated acceptor strand and 10 nM donor strand were added to a 10 nM donor strand solution, so the donor concentration remains constant. Aliquots were added until the fluorescence intensity remained constant within experimental error. There were typically 10 points (at least seven points) in the titration curves, from point zero to saturation. In this process, the competitor strand will break the pseudoknot and form a reference structure, whose free energy can be predicted with the INN-HB model (39) combined with hairpin (60) and dangling end (61, 62) free energy parameters (see the Supporting Information).

Following Gelfand et al. (53), for each titration point, the solution to be measured at pH 6.0 or 7.0 was annealed for 3 min at 75 °C in a water bath and then equilibrated at 37 °C for at least 15 min in a 4 mm × 4 mm quartz cuvette in a HORIBA Jobin Yvon Fluorolog-3 spectrofluorometer. To check for equilibrium, fluorescence intensity was measured for 150 s at intervals of 5 min. If no change was observed between two measurements, then the average over the last 150 s was taken as the fluorescence intensity of the titration point. Fluorescence was excited at 494 nm with a 2 nm band-pass, and emission was measured at the peak of the emission, 520 nm, with a 1 nm band-pass.

For titration points in buffer at pH 8.0, the annealing process was omitted to avoid hydrolysis, and the measuring time for fluorescence intensity was shortened to 30 s to avoid photo-bleaching. The time for equilibrating was at least 30 min. To check for equilibrium, fluorescence intensity was measured at intervals of 10 min. All other operations were the same as in buffers at pH 6.0 or 7.0.

**Fluorescence Competition Assay (FCA).** Duplex formation quenches the fluorescence by up to 30% of a 3'-dangling fluorescein directly adjacent to a terminal G–C base pair. Thus, a fluorescence competition assay does not require a non-nucleotide quencher. This permits a fluorescence competition assay in which only the short competition strand is labeled, which is more economical than synthesizing fluorescently labeled pseudoknots (Figure 2B). In this case, the equilibrium is forced to shift to the reference structure with an increase in the pseudoknot concentration. The free energy of this reference structure can be calculated by combination of optical melting results with duplex 5'GAACAAACGG/3'AACUUGUUUGF (Table 1) and the INN-HB model (39) with hairpin loop (60) and coaxial stacking (63) free energy parameters (see the Supporting Information).

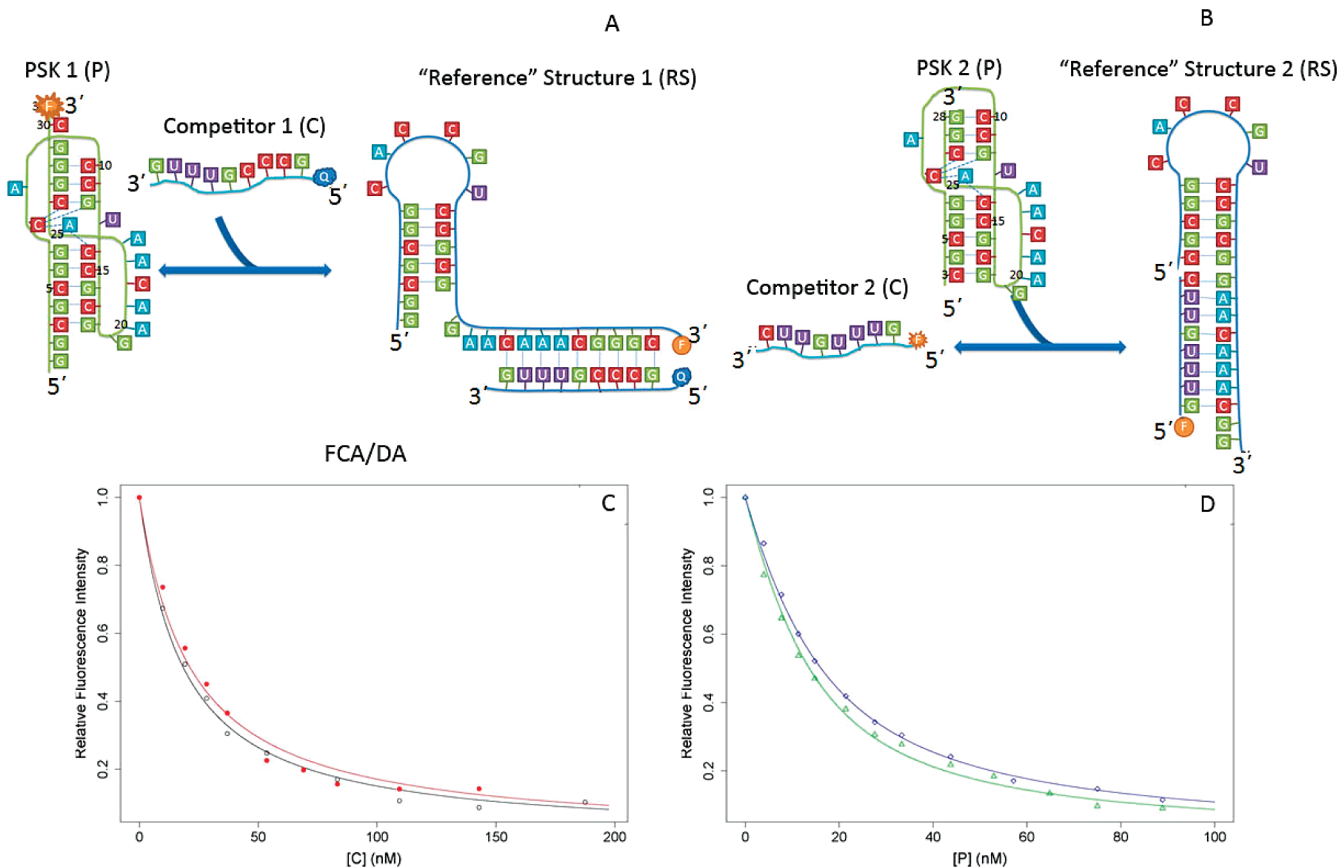


FIGURE 2: (A) Diagram of FCA/DA. PSK 1 is labeled with a fluorescence donor, fluorescein, at the 3' end, and competitor 1 is labeled with a fluorescence quencher at the 5' end. As the competitor is titrated into the pseudoknot, stem 2 of the pseudoknot will be broken and form a reference structure. The fluorescein and the quencher are close, and fluorescence quenching by FRET will be observed. (B) Diagram of FCA. Competitor 2 is labeled with fluorescein at the 5' end. PSK 2 is titrated into the competitor solution, and stem 2 of the pseudoknot will be broken; the complex is formed, and the fluorescence will be quenched by the adjacent base pair. Note that the 5' nucleotide of PSK 2 is labeled as C3 to match up with 437D PSK (Figure 1B). (C) Titration curves and fitting for FCA/DA. The PSK 1 concentration is 10 nM, and [C] is the concentration of the titrated competitor 1 (panel A). (D) Titration curves and fitting for FCA. The competitor 2 concentration is 2 nM, and [P] is the concentration of PSK 2 (panel B). These titrations were conducted at 37 °C in 1.0 M NaCl, 20 mM sodium cacodylate, and 0.5 mM Na<sub>2</sub>EDTA (pH 7.0). Two separate titrations are shown for each type of assay.

Because the 5' end dangling GG used for crystallography is not related to the competition and it is expected to stabilize stem 1 of the pseudoknot by only 0.4 kcal/mol (61, 62, 64), it was eliminated to give the construct called PSK 2 (Figure 2B). Note, however, that the 5' nucleotide is labeled C3 to match with the 437D PSK numbering in Figure 1B.

In FCA experiments, the initial solution was the fluorescein-labeled competitor 2 at 2 nM in 250 μL of standard melting buffer and its fluorescence intensity was measured for the zero point of titration. Aliquots of a mixture of concentrated pseudoknot and 2 nM competitor 2 were added. Then, the solution was annealed at 75 °C for 3 min and equilibrated for at least 15 min at 37 °C. The relative fluorescence intensity was measured in the same way as in FCA/DA experiments except with a 4 nm emission band-pass.

**Calculating Pseudoknot Stability from FCA and FCA/DA Data.** Below is the derivation of the equation for fluorescence intensity as a function of solution composition for FCA titrations. The derivation for FCA/DA is similar. Figure 3 illustrates the equilibria involved in the calculations.

Relative to fluorescein, the fluorescence from nucleotides is very low and can be neglected. The fluorescence comes from fluorescein in the free competitor single strand (C) or reference structure (RS). Therefore, the fluorescence intensity,  $F$ , is

$$F = f_C[C] + f_{RS}[RS] \quad (1)$$

where  $f_C$  and  $f_{RS}$  are the fluorescence efficiencies for the competitor and reference structure, respectively,  $[C]$  is the

concentration of free competitor strand, and  $[RS]$  is the concentration of the reference structure. The total concentration of the competitor strand is

$$[C]_T = [C] + [RS] \quad (2a)$$

$$[C] = [C]_T - [RS] \quad (2b)$$

From eqs 1 and 2

$$\begin{aligned} F &= f_C([C]_T - [RS]) + f_{RS}[RS] \\ &= f_C[C]_T + (f_{RS} - f_C)[RS] \end{aligned} \quad (3)$$

In the solution, the pseudoknot RNA could be in different forms: pseudoknot ([P] for the concentration), reference structure, and hairpin ([H] for its concentration). Therefore, the total concentration of pseudoknot RNA can be expressed as

$$[P]_T = [P] + [H] + [RS] \quad (4a)$$

$$[P] + [H] = [P]_T - [RS] \quad (4b)$$

Other possible conformations of the pseudoknot could be added to the equation if needed. The equilibrium constant,  $K_c$ , for the competition (Figure 3A) can be written as

$$K_c = \frac{[RS]}{[C][P]_T} \quad (5)$$

Table 1: Thermodynamics of Model Duplexes for the Free Energy of Dangles, Including Fluorophores<sup>a</sup>

Duplex	$T_m^{-1}$ vs $\ln(C_T/4)$ plots				Average of melt curve fits				Sequence of dangle or modification	$-\Delta G_{37}^0$ (kcal/mol) For dangle or modification
	$-\Delta H^\ddagger$ (kcal/mol)	$-\Delta S^\ddagger$ (eu)	$-\Delta G_{37}^0$ (kcal/mol)	$T_m^b$ (°C)	$-\Delta H^\ddagger$ (kcal/mol)	$-\Delta S^\ddagger$ (eu)	$-\Delta G_{37}^0$ (kcal/mol)	$T_m^b$ (°C)		
5'CUGGC3' 3'GACCG5'	57.82±1.53 (45.58±4.92)	166.69±5.00 (125.1±15.15)	6.13±0.03 (6.78±0.26)	34.9 (38.7)	57.90±6.92	166.77±23.05	6.18±0.17	35.1	/	/
5'CUGGCF3' 3'GACCGQ5'	59.81±5.21	164.19±16.23	8.89±0.22	49.7	58.24±1.99	159.24±6.42	8.85±0.20	49.9	CF3' GQ5'	2.76±0.19
5'GACAAG3' 3'CUGUUC5'	66.95±6.78 (47.97±4.90)	198.18±22.23 (136.5±15.04)	5.48±0.20 (5.62±0.25)	32.2 (31.3)	68.98±18.45	204.29±60.00	5.62±0.32	33.0	/	/
5'GACAAGGC3' 3'CUGUUC5'	89.41±9.55	263.12±30.37	7.80±0.21	41.5	77.83±23.70	225.59±75.44	7.86±0.43	42.4	5'GGCF 3'C	2.32±0.10
5'GAACAAACGG3' 3'AACUUGUUUG5'	93.52±4.71	262.50±14.36	12.10±0.26 (11.74±0.26)	56.6	88.54±3.30	247.34±10.25	11.83±0.15	56.7	/	/
5'GAACAAACGG3' 3'AACUUGUUUGF5'	95.68±3.29	266.86±9.99	12.92±0.19	59.2	95.48±9.38	266.24±28.50	12.91±0.55	59.2	F5'	0.82±0.20

<sup>a</sup>The buffer consists of 1.0 M NaCl, 20 mM sodium cacodylate, and 0.5 mM Na<sub>2</sub>EDTA (pH 7.0). Values from  $T_m^{-1}$  plots were obtained from fitting to the equation  $T_m^{-1} = (R/\Delta H^\ddagger) \ln([C]_T/4) + \Delta S^\ddagger/\Delta H^\ddagger$ . Values in parentheses are predicted from the INN-HBB model (39) with double-dangling end parameters (61, 62). <sup>b</sup> $T_m$  at a total strand concentration of  $1 \times 10^{-4}$  M.

From eqs 2, 4, and 5

$$K_c = \frac{[RS]}{([C]_T - [RS])([P]_T - [RS])} \quad (6)$$

Equation 6 can be rewritten as

$$[RS]^2 - \left( [C]_T + [P]_T + \frac{1}{K_c} \right) [RS] + [C]_T [P]_T = 0 \quad (7)$$

Solving for [RS] gives

$$[RS] = \frac{1}{2} \left[ [C]_T + [P]_T + \frac{1}{K_c} \pm \sqrt{\left( [C]_T + [P]_T + \frac{1}{K_c} \right)^2 - 4[C]_T [P]_T} \right] \quad (8)$$

Because [RS] cannot be larger than [C]<sub>T</sub> or [P]<sub>T</sub>, the only valid solution is

$$[RS] = \frac{1}{2} \left[ [C]_T + [P]_T + \frac{1}{K_c} - \sqrt{\left( [C]_T + [P]_T + \frac{1}{K_c} \right)^2 - 4[C]_T [P]_T} \right] \quad (9)$$

Via substitution of [RS] in eq 3 by eq 9, the fluorescence intensity can be expressed as

$$F = f_C [C]_T + \frac{f_{RS} - f_C}{2} \left[ [C]_T + [P]_T + \frac{1}{K_c} - \sqrt{\left( [C]_T + [P]_T + \frac{1}{K_c} \right)^2 - 4[C]_T [P]_T} \right] \quad (10)$$

The value of  $f_C$  is known from the fluorescence of the competitor solution; [C]<sub>T</sub> and [P]<sub>T</sub> are the concentrations added,

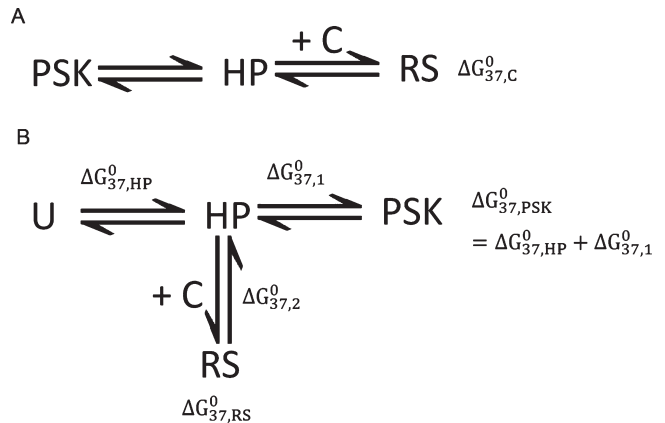


FIGURE 3: Equilibria discussed in the text. (A) Measurement provides  $K_c$  for competitor, C, binding to pseudoknot, PSK, and thus  $\Delta G_{37,C}^0 = -RT \ln K_c$ . (B) Calculation of the free energy,  $\Delta G_{37,PSK}^0$ , for forming a pseudoknot from unfolded RNA. The value of  $\Delta G_{37,HP}^0$  is calculated from nearest-neighbor parameters (39, 60);  $\Delta G_{37,1}^0 \approx \Delta G_{37,2}^0 - \Delta G_{37,C}^0$ , where  $\Delta G_{37,2}^0$  is calculated from optical melting results and nearest-neighbor parameters (see the Supporting Information).

so the titration curve was fit to  $f_{RS}$  and  $K_c$  by the Newton-Gaussian method as implemented in Statistical Analysis System (SAS) from SAS Institute Inc.

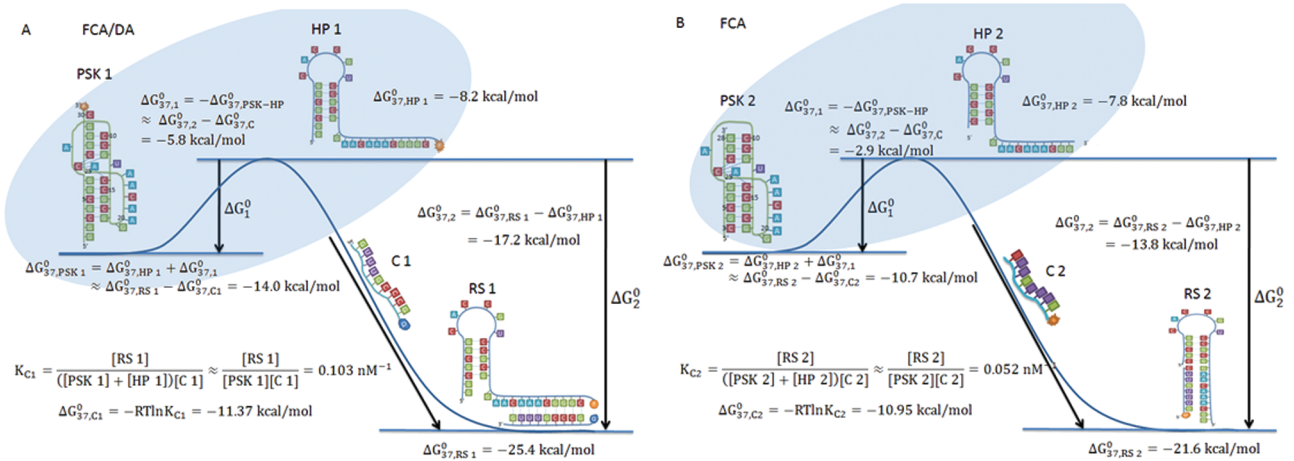
Figure 4B is a free energy diagram for the competition. In the solution, there is the equilibrium between pseudoknot and hairpin, with equilibrium constant  $K_1$ :

$$K_1 = \frac{[P]}{[H]} \quad (11a)$$

$$[P] = K_1 [H] \quad (11b)$$

The free energy difference between pseudoknot and hairpin is  $\Delta G_1^0$ :

$$\Delta G_1^0 = \Delta G_{PSK}^0 - \Delta G_{HP}^0 \quad (12)$$



Experiment	pH	$K_C (10^9 M^{-1})$	$\ln K_C$	$\Delta G_{37,C}^0$ (kcal/mol)	$\Delta G_{37,RS}^0$ (kcal/mol) <sup>a</sup>	$\Delta G_{37,HP}^0$ (kcal/mol) <sup>a</sup>	$\Delta G_{37,2}^0$ (kcal/mol)	$\Delta G_{37,1}^0$ (kcal/mol)	$\Delta G_{37,PSK}^0$ (kcal/mol)	$\Delta G_{37,437D\ PSK}^0$ (kcal/mol)	$\Delta G_{37,437D\ PSK-HP}^0$ (kcal/mol)
FCA/DA for PSK 1	6.0	$0.055 \pm 0.003$	$17.82 \pm 0.06$	$-10.95 \pm 0.06$	$-25.4 \pm 0.4$	$-8.2 \pm 0.2$	$-17.2 \pm 0.4$	$-6.3 \pm 0.4$	$-14.5 \pm 0.4$	$-12.2 \pm 0.4$	$4.0 \pm 0.4$
	7.0	$0.103 \pm 0.001$	$18.45 \pm 0.01$	$-11.37 \pm 0.01$	$-25.4 \pm 0.4$	$-8.2 \pm 0.2$	$-17.2 \pm 0.4$	$-5.8 \pm 0.4$	$-14.0 \pm 0.4$	$-11.7 \pm 0.4$	$3.5 \pm 0.4$
	8.0	$0.320 \pm 0.001$	$19.58 \pm 0.01$	$-12.07 \pm 0.01$	$-25.4 \pm 0.4$	$-8.2 \pm 0.2$	$-17.2 \pm 0.4$	$-5.1 \pm 0.4$	$-13.3 \pm 0.4$	$-11.0 \pm 0.4$	$2.8 \pm 0.4$
FCA for PSK 2	7.0	$0.052 \pm 0.001$	$17.77 \pm 0.02$	$-10.95 \pm 0.01$	$-21.6 \pm 0.3$	$-7.8 \pm 0.2$	$-13.8 \pm 0.2$	$-2.9 \pm 0.2$	$-10.7 \pm 0.2$	$-11.1 \pm 0.2$	$2.9 \pm 0.2$

<sup>a</sup>the nearest neighbor parameters used here are from experiments at pH 7.

FIGURE 4: (A and B) Free energy diagrams for FCA/DA and FCA, respectively, including the calculations for the free energy changes. There is the equilibrium between pseudoknot (PSK) and hairpin (HP) in solution with free energy difference  $\Delta G_1^0$  and the equilibrium among folded hairpin (HP), competitor (C), and reference structure (RS) with free energy difference  $\Delta G_2^0$ . The  $\Delta G_{37,C}^0$  is the measured free energy change for the binding of competitor to pseudoknot/hairpin to give the reference structure.  $\Delta G_{37,RS}^0$  is the calculated free energy change for formation of RS from the random coil hairpin sequence and competitor (see the Supporting Information, I).  $\Delta G_{37,PSK}^0$  is the free energy for forming PSK 1 or 2 from unfolded RNA. If  $-\Delta G_2^0 - \Delta G_C^0 > 1.2$  kcal/mol at 37 °C, then  $\Delta G_1^0 = \Delta G_2^0 - \Delta G_C^0$  and  $\Delta G_{PSK}^0 = \Delta G_{RS}^0 - \Delta G_C^0$ . In the table,  $\Delta G_{37,437D\ PSK}^0$  is the free energy for forming 437D PSK from unfolded RNA. This is  $\Delta G_{37,PSK}^0$  made less favorable by 2.32 kcal/mol to account for the 3' GCF dangling end or  $\Delta G_{37,PSK_2}^0$  made more favorable by 0.4 kcal/mol to account for the 5' GG dangling end on 437D PSK (see the Supporting Information, II); the sequence of 437D PSK is shown in Figure 1B. The  $\Delta G_{37,437D\ PSK-HP}^0$  is the free energy change for the transition from 437D PSK to the stem 1 hairpin; i.e. the transition is in the direction opposite that for  $\Delta G_{PSK}^0$ . All the free energies are for 37 °C. The error for the FCA/DA result is larger than for the FCA result because fluorescein was attached to the pseudoknot, which introduces an additional source of error. The table summarizes the results from the two versions of competition assays.

where  $\Delta G_{PSK}^0$  is the free energy change for forming the pseudoknot from random coil and  $\Delta G_{HP}^0$  is the free energy change for forming the hairpin from random coil.

There is also the equilibrium among hairpin, competitor, and reference structure, with equilibrium constant  $K_2$ :

$$K_2 = \frac{[RS]}{[C][H]} \quad (13)$$

The free energy difference between reference structure and hairpin is  $\Delta G_2^0$ :

$$\Delta G_2^0 = \Delta G_{RS}^0 - \Delta G_{HP}^0 \quad (14)$$

where  $\Delta G_{RS}^0$  is the free energy change for forming the reference structure from random coil.

Substituting [P] in eq 5 by eq 11 gives

$$K_c = \frac{[RS]}{[C][H](K_1 + 1)} = \frac{K_2}{K_1 + 1} \quad (15)$$

Therefore

$$K_1 = \frac{K_2}{K_c} - 1 \quad (16)$$

Relating the equilibrium constants to free energy changes

$$K_2 = e^{-\Delta G_2^0/RT} \quad (17)$$

$$K_c = e^{-\Delta G_C^0/RT} \quad (18)$$

where  $R$  is the gas constant (1.987 cal K<sup>-1</sup> mol<sup>-1</sup>) and  $T$  is the absolute temperature. Therefore

$$K_1 = \frac{e^{-\Delta G_2^0/RT}}{e^{-\Delta G_C^0/RT}} - 1 = e^{-(\Delta G_2^0 - \Delta G_C^0)/RT} - 1 \quad (19)$$

$$\Delta G_1^0 = -RT \ln[e^{-(\Delta G_2^0 - \Delta G_C^0)/RT} - 1] \quad (20)$$

If  $-(\Delta G_2^0 - \Delta G_C^0) > 1.2$  kcal/mol, then

$$\Delta G_1^0 = \Delta G_2^0 - \Delta G_C^0 \quad (21)$$

Substituting  $\Delta G_2^0$  in eq 21 by eq 14 gives

$$\Delta G_1^0 = \Delta G_{RS}^0 - \Delta G_{HP}^0 - \Delta G_C^0 \quad (22)$$

Substituting  $\Delta G_1^0$  in eq 12 by eq 22 gives

$$\Delta G_{PSK}^0 = \Delta G_{RS}^0 - \Delta G_C^0 \quad (23)$$

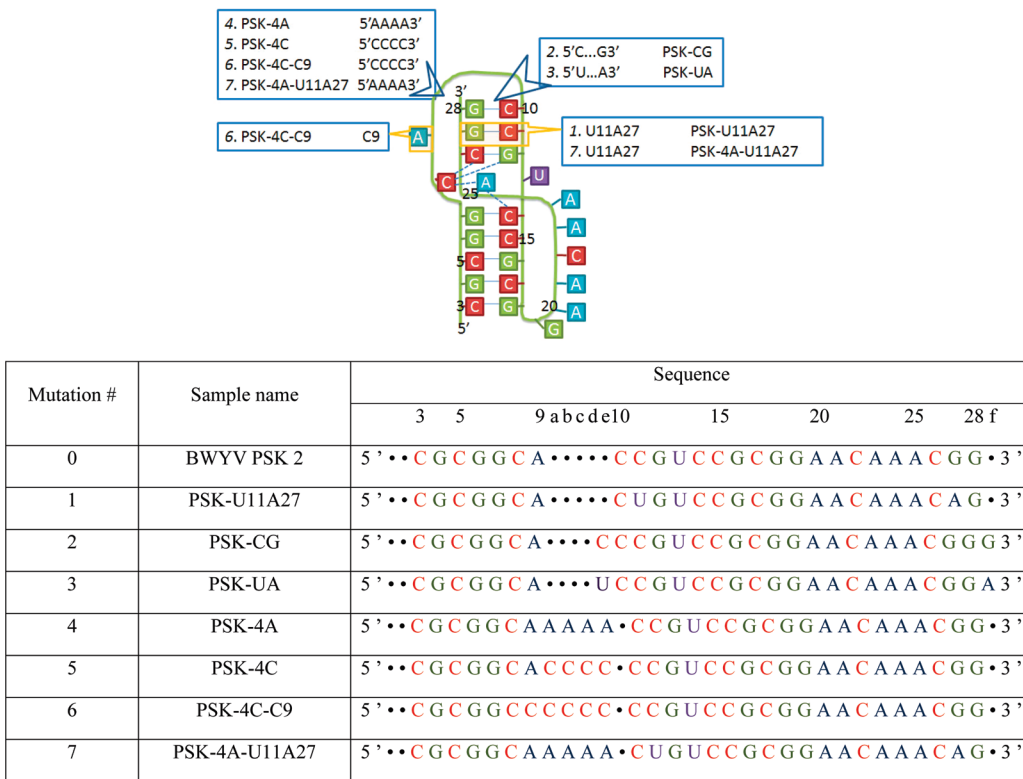


FIGURE 5: Mutations for BWYV PSK 2 in the stem 2–loop 1 region. The empty blue arrowheads denote insertions of a base or base pair (listed behind the arrow). The yellow boxes denote mutations of the base or base pair. The table lists the sequences and names of the mutations. Note that the sequences start at nucleotide 3 to maintain the nucleotide number in Figures 1B and 2A. For SPM and NUPACK predictions, U13 and A25 are assumed to form a Watson–Crick base pair that coaxially stacks on G7–C14.

$\Delta G_{RS}^0$  and  $\Delta G_{HP}^0$  can be calculated with the combination of melting model duplexes (Table 1) and the INN-HB model (39, 40) with hairpin loop (60), dangling end (61, 62), and coaxial stacking (63) free energy parameters (see the Supporting Information).  $\Delta G_C^0$  is measured with the FCA titration. Thus, the free energy change from hairpin to pseudoknot,  $\Delta G_1^0$ , and the free energy change for forming the pseudoknot from the unfolded RNA,  $\Delta G_{PSK}^0$ , can be determined.

## RESULTS

**Free Fluorescein Does Not Interact with RNA Single Strands or Duplex.** To test for binding between free fluorescein and RNA, the fluorescence of free fluorescein titrated into standard melting buffer (buffer/fluorescein) was compared to the fluorescence of free fluorescein titrated into RNA single strand (5'GAACAAACGG3') or duplex (5'GAACAAACGG/3'CUUGUUUG) (buffer/oligonucleotide/fluorescein) at 100 nM. Presumably, intercalation of the dye would change the emission profile or the intensity of emission. In titrations with 2, 20, 100, and 1000 nM fluorescein, however, the fluorescence from the buffer/fluorescein solution was always within experimental error of the fluorescence from the buffer/oligonucleotide/fluorescein solution.

**Fluorescein Attached to an Oligonucleotide Interacts with the RNA.** The fluorescence of fluorescein covalently linked to the 5' end of an oligonucleotide is quenched upon duplex formation (Figure 2B and 2D). Evidently, fluorescein interacts with the helix, presumably by stacking and possibly forming hydrogen bonds. UV melting experiments reveal that covalently linked fluorescein stabilizes a duplex (Table 1), which also indicates interaction between fluorescein and the helix.

A fluorescein–quencher pair also stabilizes a duplex (Table 1). These interactions must be taken into account when the free energy for the reference structure with a pseudoknot is calculated. Values and increments from  $T_m^{-1}$  versus  $\ln([C]_T/4)$  plots in Table 1 were used for the calculation of pseudoknot free energy.

**FCA/DA and FCA Methods Give Similar Results.** Panels C and D of Figure 2 show fluorescence titrations for FCA/DA on PSK 1 and FCA on PSK 2, respectively, along with the fitted curves for each experiment at pH 7.0. The free energy diagrams including free energy change calculations are shown in panels A and B of Figure 4, respectively. To compare with previous measurements on 437D PSK (44, 45), the predicted free energy increment (62) for the two 5' dangling G residues on 437D PSK (Figure 1B) was included in the predicted  $\Delta G_{37,HP}^0$  for the FCA experiment, and for the FCA/DA experiment, the total free energy of the pseudoknot was made less favorable by the free energy increment for the 3' dangling GCF in PSK 1 (see the Supporting Information, II). The table in Figure 4 summarizes the results from the two versions of fluorescence competition assays. The two titration methods give similar results for  $\Delta G_{37,437D}^0$  PSK and  $\Delta G_{37,437D}^0$  PSK-HP, even though they employ very different concentrations of the pseudoknot and different competitors. The results suggest that intermolecular interactions of the pseudoknot sequences are negligible under the experimental conditions.

**FCA/DA Results at Different pHs Agree with Expectations from the Crystal Structure.** The table in Figure 4 lists the free energy changes of the pseudoknot to stem 1 hairpin for 437D PSK ( $\Delta G_{37,437D}^0$  PSK-HP) measured by FCA/DA at pH 6.0, 7.0, and 8.0 and 37 °C. The values are 4.0, 3.5, and 2.8 kcal/mol, respectively. The pseudoknot is destabilized as the pH increases.

Table 2: Thermodynamic Parameters for BYWV PSK 2 and Its Mutants<sup>a</sup>

motif	$\Delta G_{37}^0$ (kcal/mol)							$\Delta \Delta G_{37}^0$ (kcal/mol) for mutation from BWYV PSK 2								
	INN-HB		FCA			SPM <sup>d</sup>		NUPACK <sup>d</sup>			FCA		SPM		NUPACK	
	HP <sup>b</sup>	RS	competition <sup>c</sup>	PSK–HP	PSK	PSK–HP	PSK	PSK–HP	PSK	PSK–HP	PSK	PSK–HP	PSK	PSK–HP	PSK	
BWYV PSK 2	-7.8	-21.6	-10.95	2.9	-10.7	3.7	-11.5	3.2	-11.0	-	-	-	-	-	-	
PSK-U11A27	-7.8	-21.6	-12.14	1.7	-9.5	2.3	-10.1	1.8	-9.6	-1.2	1.2	-1.4	1.4	-1.4	1.4	
PSK-CG	-8.2	-23.8	-12.53	3.1	-11.3	6.6	-14.8	6.1	-14.3	0.2	-0.6	2.9	-3.3	2.9	-3.3	
PSK-UA	-8.2	-22.0	-11.70	2.1	-10.3	5.7	-13.9	5.2	-13.4	-0.8	0.4	2.0	-2.4	2.0	-2.4	
PSK-4A	-7.8	-21.6	-11.97	1.8	-9.6	2.7	-10.5	2.8	-10.6	-1.1	1.1	-1.0	1.0	-0.4	0.4	
PSK-4C	-7.8	-21.6	-12.29	1.5	-9.3	2.7	-10.5	2.8	-10.6	-1.4	1.4	-1.0	1.0	-0.4	0.4	
PSK-4C-C9	-6.7	-20.5	-12.18	1.6	-8.3	3.8	-10.5	3.9	-10.6	-1.3	2.4	0.1	1.0	0.7	0.4	
PSK-4A-U11A27	-9.2	-23.0	-12.26	1.5	-10.7	-0.1	-9.1	0	-9.2	-1.4	0	-3.8	2.4	-3.2	1.8	

<sup>a</sup>The sequence and secondary structure of the oligonucleotides are shown in Figure 5. All the measurements were conducted by FCA, in 1.0 M NaCl, 20 mM sodium cacodylate, and 0.5 mM Na<sub>2</sub>EDTA (pH 7.0). <sup>b</sup>See the Supporting Information for predictions of hairpin stability. <sup>c</sup>The error from the FCA experiment is within  $\pm 0.01$  kcal/mol. <sup>d</sup>In SPM and NUPACK predictions, it is assumed that U13 forms a Watson–Crick base pair with A25 and coaxially stacks with the G7-C14 base pair (see the Supporting Information for calculations).

These results agree with expectations from the BWYV pseudoknot crystal structure (PDB entry 437D). In the crystal structure, there is a quadruple-base interaction with a hydrogen bond between protonated C8 and G12 at the joint of stems 1 and 2 (Figure 1C). An increasing pH will weaken this interaction and destabilize the pseudoknot. The FCA/DA results, however, give a destabilization of  $1.2 \pm 0.6$  kcal/mol between pH 6.0 and 8.0 at 37 °C, whereas previous measurements by DSC and optical melting at temperatures between 49 and 82 °C gave destabilizations of  $3.4 \pm 1.1$  and  $2.6 \pm 1.1$  kcal/mol, respectively, when extrapolated to 37 °C (44).

**FCA Measurements of the Sequence Dependence of Pseudoknot Stability.** Free energies of BWYV PSK 2 mutants in the stem 2–loop 1 region were measured by FCA. Figure 5 summarizes the mutations. Except for PSK-CG, 5'FGUUU-GUUC3' was the competition strand, i.e., the same as for PSK 2. For PSK-CG, the competition strand was 5'FCGUUGUUC3', to allow saturated binding at convenient concentrations of the pseudoknot. Table 2 lists the measured  $\Delta G_{37}^0$  values for the transition from pseudoknot to hairpin (PSK–HP) and from unfolded RNA to pseudoknot (PSK), along with predictions by the statistical polymer model (SPM) of Cao and Chen (42) and the NUPACK model (33). The value of  $\Delta G_{37,PSK-HP}^0$  shows the relative stability of the pseudoknot to the stem 1 hairpin, which is important for the function of many pseudoknots (18, 27, 30, 31). Some mutations make the free energy of the pseudoknot more favorable, but it may not make the pseudoknot more stable relative to the corresponding hairpin and vice versa. Table 2 also lists the changes ( $\Delta \Delta G_{37}^0$ ) of  $\Delta G_{37}^0$  for the transitions due to mutations to PSK 2. This provides insight into the effects of different factors on pseudoknot stability.

## DISCUSSION

Pseudoknots are present in many RNAs and important for many functions (1–23). It is difficult to predict pseudoknot structures by free energy minimization, however, because the inclusion of pseudoknots greatly complicates algorithms for predicting secondary structure (32–37, 65) and little is known about the sequence dependence of pseudoknot stability. Here, two methods are used for measuring the stability of pseudoknots, and results are presented for several sequence variations. The experiments were conducted at 37 °C, which is human body temperature.

The two fluorescence titration methods each have advantages and disadvantages. For both, the concentration of the pseudoknot required for the titration can be manipulated by altering the sequence and length of the competition strand. They both can work at nanomolar oligonucleotide concentrations, which allows studies of sequence dependence with only small quantities of RNA and avoids potential problems from intermolecular interactions of the pseudoknot sequences. The FCA/DA method provides a large change in fluorescence intensity, and the concentration of pseudoknot RNA remains the same during the titration. That can avoid some complications due to possible intermolecular interactions. The FCA/DA method, however, requires the synthesis of pseudoknot RNA with a fluorescent tag, which makes the experiment more expensive. In FCA, the concentration of pseudoknot RNA can be as high as hundreds of nanomolar, but it does not require fluorescent modification of the pseudoknot. Thus, the pseudoknot can be made by either chemical synthesis or T7 transcription (66).

**Comparison of BWYV Pseudoknot Free Energies from Different Experimental Methods.** The 437D PSK thermodynamics have been measured by Nixon and Giedroc using UV melting and DSC (44) and by Soto et al. using UV melting (45). Nixon and Giedroc conducted the measurement in 0.5 M K<sup>+</sup> buffer (pH 6.0, 7.0, and 8.0) with a pseudoknot concentration of 34.8 μM. Soto et al. used 0.5 M Na<sup>+</sup> buffer (pH 7.0) with ~1.8 μM pseudoknot and reported their results for  $\Delta H^0$  and  $T_m$ , which allows  $\Delta G_{37}^0$  to be calculated from the relation  $\Delta G_{37}^0 = \Delta H^0 - 310.15\Delta H^0/T_m$ . Both groups obtained their thermodynamics from deconvoluting UV melting or DSC curves with overlapping transitions. They assign the melting curves in the same way, i.e., as three two-state transitions in the thermal denaturation: F → PK → S1 → U, where F is a completely folded pseudoknot, including tertiary interactions, PK is the secondary structure of the pseudoknot, S1 is the stem 1 hairpin corresponding to the pseudoknot, and U is the completely unfolded pseudoknot. The sum of the first two transitions (F → PK → S1) corresponds to the 437D PSK–HP transition measured here. The sum of  $\Delta G_{37}^0$  for the F → PK and PK → S1 transitions is listed under  $\Delta G_{37}^0$  for the 437D PSK–HP transition in Table 3. As Soto et al. stated, there are ~10 °C differences in the melting temperatures for both the F → PK and PK → S1 transitions between the two reports, which could be due to the different cations (67–69). This produces a difference of 1.6 kcal/mol in  $\Delta G_{37,PSK-HP}^0$  between the measurements of the two groups.

Table 3: Thermodynamic Parameters for 437D PSK by Different Methods

method	cation	$\Delta G_{37}^0$ (kcal/mol)		
		stem 1 HP (U→HP)	437D PSK (U→PSK)	437D PSK–HP (PSK→HP)
FCA/DA <sup>a</sup>	1 M Na <sup>+</sup>	−8.2 <sup>g</sup>	−11.7	3.5
FCA <sup>a</sup>	1 M Na <sup>+</sup>	−8.2 <sup>g</sup>	−11.1	2.9
DSC <sup>b</sup>	0.5 M K <sup>+</sup>	−8.3 <sup>h</sup>	−13.3	5.0
UV melting <sup>b</sup>	0.5 M K <sup>+</sup>	−7.8 <sup>h</sup>	−12.9	5.1
UV melting <sup>c</sup>	0.5 M Na <sup>+</sup>	−8.4 <sup>h</sup>	−15.1	6.7
polymer model <sup>d</sup>	1 M Na <sup>+</sup>	−8.2 <sup>g</sup>	−11.9	3.7
NUPACK <sup>e</sup>	1 M Na <sup>+</sup>	−8.2 <sup>g</sup>	−11.4	3.2
Kinefold <sup>f</sup>	1 M Na <sup>+</sup>	−7.3 <sup>f</sup>	−8.9	1.6

<sup>a</sup>Buffer: 1.0 M NaCl, 20 mM sodium cacodylate, and 0.5 mM Na<sub>2</sub>EDTA (pH 7.0). <sup>b</sup>From ref 44; buffer: 0.5 M KCl and 0.010 M Mops (pH 7.0). <sup>c</sup>From ref 45; buffer: 0.5 M NaCl and 0.010 M Mops (pH 7.0). <sup>d</sup>From ref 42. <sup>e</sup>From ref 33. <sup>f</sup>From ref 37; predictions generated at <http://kinefold.curie.fr/>. <sup>g</sup>Predicted from the INN-HB model (39) with hairpin loop (60) and dangling end (61, 62) parameters. <sup>h</sup>Measured.

The 437D PSK sequence (Figure 1B) has different termini compared to the sequences used for FCA/DA and FCA experiments (Figure 2). As described in Results, the FCA/DA and FCA results were adjusted to account for these differences (see the Supporting Information, II). The resulting free energies for 437D PSK, stem 1 hairpin, and 437D PSK–HP transitions are listed in Table 3. The average value of  $\Delta G_{37}^0$  measured by FCA/DA and FCA for the 437D PSK–HP transition in 1.0 M Na<sup>+</sup> is 3.2 kcal/mol. This value is 2.4 kcal/mol more favorable than the value from averaging UV melting and DSC experiments in 0.5 M Na<sup>+</sup> or K<sup>+</sup> buffer. The higher cation concentration is expected to stabilize the RNA pseudoknot structure relative to the corresponding hairpin, but it apparently destabilizes it.

As the pH was increased from 6.0 to 7.0 and from 7.0 to 8.0, the pseudoknot was destabilized by 0.5 ± 0.4 and 0.7 ± 0.4 kcal/mol for FCA/DA measurements, by 1.2 ± 1.2 and 1.3 ± 0.5 kcal/mol for UV melting measurements, and by 2.3 ± 1.2 and 1.1 ± 0.5 kcal/mol for DSC measurements, respectively (44). FCA/DA, UV melting, and DSC results agree that an increasing pH destabilizes the BWYV pseudoknot as expected from the crystal structure (PDB entry 437D).

A difference between the fluorescence competition assay (FCA and FCA/DA) experiments and thermal melting (UV melting and DSC) is the temperature of the experiment. The FCA/DA and FCA experiments were conducted at 37 °C, while  $\Delta G_{37}^0$  values of the 437D PSK from UV melting and DSC were extrapolated from the melting temperatures, which were ~60 and ~80 °C for the first two transitions, respectively, at 0.5 M Na<sup>+</sup> or K<sup>+</sup>. In the extrapolations to 37 °C, the enthalpy and entropy changes were considered temperature-independent; i.e., the heat capacity change ( $\Delta C_p^0$ ) was assumed to be zero. In general, however, the unfolding of RNA is accompanied by a non-zero  $\Delta C_p^0$ , which can be as large as hundreds of calories per kelvin per mole per base pair or base triple (70). If  $\Delta C_p^0$  is approximated as a temperature-independent constant, then

$$\Delta H_T^0 = \Delta H_{T_0}^0 + \Delta C_p^0(T - T_0) \quad (24)$$

$$\Delta S_T^0 = \Delta S_{T_0}^0 + \Delta C_p^0 \ln(T/T_0) \quad (25)$$

$$\begin{aligned} \Delta G_T^0 &= \Delta H_{T_0}^0 - T\Delta S_{T_0}^0 + \Delta C_p^0[(T - T_0) \\ &\quad - T \ln(T/T_0)] \end{aligned} \quad (26)$$

Thus, if  $\Delta C_p^0$  is taken into consideration, then the extrapolated thermodynamic parameters will vary. For example, a short self-complementary duplex (5'CCGG)<sub>2</sub> has a  $\Delta C_p^0$  of −382 cal K<sup>−1</sup> mol<sup>−1</sup> for folding (58), and  $\Delta G_{37}^0$  is 1.0 kcal/mol less favorable when taking  $\Delta C_p^0$  into account than without it if  $\Delta G_{37}^0$  is extrapolated from 80 °C (71). Optical melting of the BWYV pseudoknot in different Na<sup>+</sup> concentrations provides results at different temperatures (45). While the error limits on  $\Delta H_T^0$  do not allow a reliable value for  $\Delta C_p^0$  to be determined, linear least-squares fittings of listed  $\Delta H_T^0$  values versus  $T_m$  at 40, 74, 120, 204, and 504 mM Na<sup>+</sup> for F → PK ( $T_m$  range of 48–67 °C), PK → S1 ( $T_m$  range of 63–84 °C), and S1 → U ( $T_m$  range of 81–92 °C) transitions provide  $\Delta C_p^0$  estimates of −700, −300, and −20 cal K<sup>−1</sup> mol<sup>−1</sup> for unfolding, respectively (Supporting Information). If these  $\Delta C_p^0$  values are included, then the average  $\Delta G_{37}^0$  calculated by eq 26 for the PSK–HP transition from UV melting and DSC experiments in 0.5 M Na<sup>+</sup> or K<sup>+</sup> buffer will be less favorable by 1.4 kcal/mol relative to the average  $\Delta G_{37}^0$  without considering  $\Delta C_p^0$  values. However, for the S1 → U transition, the  $\Delta G_{37}^0$  difference with  $\Delta C_p^0$  considered is within 0.1 kcal/mol of that without considering  $\Delta C_p^0$ .

There are a number of other possible reasons for differences in absolute values for  $\Delta G_{37}^0$  determined by fluorescence competition and thermal melting. Nevertheless, the increments determined by any particular method for changes in sequence or conditions should be reliable at the temperature at which the experiment was conducted.

For FCA/DA and FCA, an important source of error is the estimation of the free energy for the reference structure. Here, the stem 1 hairpin is an important part of the reference structure. For 437D PSK, the stability of the stem 1 hairpin is estimated from the INN-HB model (39) combined with hairpin loop (60) and dangling end (61, 62) free energy parameters to be −8.2 kcal/mol at 37 °C. Using the  $\Delta H^0$  and  $T_m$  obtained by fitting of the three thermal denaturation curves for this transition from UV melting and DSC experiments (44, 45) produced values of −8.3, −7.8, and −8.4 kcal/mol giving an average of −8.2 kcal/mol at 37 °C, consistent with the estimate from the INN-HB model (Table 3). Both calculations ignore any  $\Delta C_p^0$  contributions, but both rely on measurements of hairpins with  $T_m$  values of >60 °C (44, 45, 72, 73). Moreover, when the  $\Delta H^0$  values obtained at different salt concentrations and therefore  $T_m$  values (45) are plotted versus  $T_m$ , the apparent  $\Delta C_p^0$  is −20.4 cal K<sup>−1</sup> mol<sup>−1</sup>, which is negligible. The NUPACK program used the INN-HB model and also predicted a  $\Delta G_{37}^0$  of −8.2 kcal/mol for the stem 1 hairpin by using the latest version of free energy parameters (39, 60–62). The heuristic program, Kinefold (37), estimates the free energy of the stem 1 hairpin as −7.3 kcal/mol, which is 0.9 kcal/mol less favorable than the values from the current INN-HB model and experiments.

**Comparison of FCA Results for the BWYV Pseudoknot to Results of Computational Models.** The experimental results for pseudoknots can be compared to predictions (Table 3). For calculating the free energy of a pseudoknot (see the Supporting Information), both the SPM (42) and NUPACK (33) models consider that stem free energies are one of the main contributions, and they are estimated by the INN-HB model (39). Both models consider that the loops make unfavorable contributions to the free energy of the pseudoknot. The NUPACK model, however, counts a penalty for initiating the pseudoknot, then assigns penalty values to each base in the loop

without considering loop sequence or position, and assigns penalty values to each base pair that borders the interior of the pseudoknot, without considering the base pair type, loop–stem correlation, or tertiary interactions. Similar to Aalberts' model (26), but with volume exclusion considered, SPM calculates the entropies for the loops with a statistical mechanical polymer model that treats loops 1 and 3 differently and takes the entropies ( $\Delta S_{\text{loops}}^0$ ) as a penalty. Conformational states allowed by different lengths of stems and loops were considered. Also, the entropy for assembling the stem–loop motifs ( $\Delta S_{\text{assemble}}^0$ ) is counted as a penalty. As with the NUPACK model, loop sequence and tertiary interactions are not included. The two models predict a similar free energy for 437D PSK (Table 3). The predictions are very close to the results from FCA/DA and FCA experiments. The models predict 437D PSK is not as stable at 37 °C as measured by UV melting and DSC, however. Kinefold predicts the pseudoknot is even less stable than these models and the FCA/DA and FCA results.

**Comparison of FCA Results with INN-HB Model Predictions for Mutations in Stem 2.** As stated by Su et al. (55), the geometries of stems 1 and 2 differ significantly from a standard A-form duplex. For example, stems 1 and 2 have average propeller twists of 15° and 26°, respectively, compared to 18.6° for the A-form. The effect of the twist on stability is unclear. For the sake of simplicity, both the SPM (42) and NUPACK (33) models use the INN-HB model (39) to calculate the free energy for the stems as a component of the free energy of a pseudoknot. Theimer et al. hypothesized that the systematic deviation of pseudoknot unfolding energetics from measurements and predictions by the INN-HB model should be attributed to tertiary interactions (47). This could be tested by mutations that change only the nearest neighbors without changing tertiary interactions.

From the BWYV pseudoknot's crystal structure (PDB entry 437D), mutation of the C11-G27 base pair to a U11-A27 base pair [PSK-U11A27 (see Figure 5)] changes only two nearest-neighbor stacks in stem 2. Table 2 shows that  $\Delta\Delta G_{37,\text{PSK-HP}}^0$  and  $\Delta\Delta G_{37,\text{PSK}}^0$  for this mutation from BWYV PSK 2 are predicted to be -1.4 and 1.4 kcal/mol, respectively, by the INN-HB model as implemented in SPM and NUPACK. The FCA experimental results for  $\Delta\Delta G_{37,\text{PSK-HP}}^0$  and  $\Delta\Delta G_{37,\text{PSK}}^0$  for this mutation are -1.2 and 1.2 kcal/mol, respectively, which is within experimental error of the prediction. This is evidence of the validity of the INN-HB model in the middle of pseudoknot stem 2. Similar agreement for substituting internal base pairs in stems 1 and 2 has been reported for the T4 pseudoknot (47).

As an additional C–G or U–A base pair is added to the top of stem 2 to give PSK-CG and PSK-UA (Figure 5), SPM and NUPACK predict the free energy for the pseudoknot by adding an additional INN-HB nearest-neighbor stack (-3.3 and -2.4 kcal/mol, respectively). The FCA experiment, however, shows free energy changes of -0.6 and 0.4 kcal/mol, respectively, from this additional base pair. In the two cases, the additional base pair is less stabilizing by 2.7 and 2.8 kcal/mol, respectively, than expected. One uncertainty in this comparison is the prediction of  $\Delta G_{37}^0$  for the hairpin in the RS2 complex (see the Supporting Information). This prediction is not likely wrong by more than 1 kcal/mol, however. Similar to the hypothesis from Theimer et al. (47), a likely explanation for the difference between prediction and experiment is induced conformational changes. In an A-type RNA helix, a base pair twists the end of the duplex by 33.1° (74). As calculated by the polymer model of Aalberts and

Hodas (26), the distance between G7 and C9e/U9e (Figure 5) through the major groove of stem 2 in PSK-CG and PSK-UA is the same as the distance between G7 and C10 in BWYV PSK 2. Therefore, nucleotides in loop 1 have to twist to connect G7 and C9e or U9e in PSK-CG or PSK-UA, respectively. That could affect the tertiary interactions among C8, G12, A25, and C26 (Figure 1B,C), which stabilize the BWYV pseudoknot as much as -3.1 kcal/mol at 37 °C (75), and therefore destabilize the pseudoknot. From FCA measurements, the penalty for breaking this tertiary interaction is ~2.8 kcal/mol at 37 °C. Evidently, loop size and tertiary interactions play an important role in pseudoknot stability.

Considering only nearest-neighbor parameters,  $\Delta G_{37,\text{PSK-CG}}^0 - \Delta G_{37,\text{PSK-UA}}^0$  is predicted to be -0.9 kcal/mol. The FCA experimental results give a difference of -1.0 kcal/mol. While the INN-HB model does not predict the free energy increment from addition of another base pair to stem 2, it does predict the difference in increment between a C–G pair and an A–U pair. This is expected if the primary effect of adding a base pair is disruption of tertiary interactions.

The coincidence of the free energy from FCA/DA and FCA and predictions for 437D PSK (Table 3) also suggests the importance of tertiary interactions. The crystal structure shows U13 flipping out without forming a base pair with A25, while there is a complicated tertiary interaction among C8, G12, C26, A25, and C14 (Figure 1B,C). Therefore, the nearest neighbors will be affected because some hydrogen bonds and base stacking are lost in the structure. In predictions, U13 and A25 are paired and their nearest-neighbor free energy parameters for stacking with the G12-C26 base pair and for coaxial stacking with the G7-C14 base pair contribute to the predicted free energy. If these stacks are not included, then the pseudoknot will be predicted not to form, and only the stem 1 hairpin will be predicted to form. The predictions agree with the FCA/DA and FCA measurements, however. Apparently, the tertiary interactions compensate for the free energy loss from not forming a U13-A25 base pair. Alternatively, crystallization may trap one of two or more structures present in solution.

**Comparison of FCA Results with Predictions for Mutations in Loop 1.** While SPM (42) and NUPACK (33) use different models to estimate the penalty for pseudoknot loops, they both gave reasonable approximations for 437D PSK (Tables 2 and 3). To test the models further, the length of loop 1 was changed. Loop 1 was lengthened with different nucleotides to produce PSK-4A, PSK-4C, and PSK-4C-C9 (Figure 5 and Table 2). As Table 2 shows, increasing the size of loop 1 destabilized the pseudoknot, as predicted by SPM and NUPACK. The measured  $\Delta\Delta G_{37,\text{PSK-4A}}^0$  and  $\Delta\Delta G_{37,\text{PSK-4C}}^0$  are 1.1 and 1.4 kcal/mol, respectively, close to the predictions of 1.0 kcal/mol for either of them by SPM. The mutations are slightly more destabilizing than the NUPACK predictions of 0.4 kcal/mol for either of them. Again, the comparisons depend on the predicted  $\Delta G_{37}^0$  for the hairpin in the RS2 complex (see the Supporting Information).

Neither the SPM nor NUPACK model predicts the large PSK destabilization calculated between PSK-4C and PSK-4C-C9 (Figure 5 and Table 2). The difference may reflect an unfavorable free energy for formation of loop 1 with all C's. Hairpin loops with oligo-C sequences are unusually unstable (60, 76). Hairpin loops of C<sub>3</sub> and C<sub>6</sub> are ~1.5 and ~3.4 kcal/mol, respectively, less stable at 37 °C than other hairpin loops with the same number of nucleotides. Some of this destabilization may reflect the extra free

energy required to unstack C's, e.g., ~0.3 kcal/mol more at 37 °C for poly-C than for poly-A (77). The FCA results suggest that there may also be an oligo-C effect for the free energy for pseudoknot loops. In PSK-4C-C9, loop 1 is formed by six C's and its free energy is ~1 kcal/mol less favorable than the free energy of PSK-4A or PSK-4C. This penalty is different from the penalty for a C<sub>6</sub> hairpin loop but similar to the penalty for a C<sub>3</sub> hairpin. Obviously, the C<sub>6</sub> hairpin loop and C<sub>6</sub> pseudoknot loop 1 have different conformations. A penalty of 1.0 kcal/mol is assigned to C<sub>6</sub> pseudoknot loop 1. If this penalty is counted in SPM, then the SPM prediction will be closer to the FCA result. The results suggest that the SPM statistical model, which includes size exclusion effects, gives good agreement between predictions and experiments for loop 1.

PSK-4A-U11A27 can be considered as a mutant from PSK-U11A27 via addition of four A's to loop 1, or a mutant from PSK-4A via mutation of the C11-G27 base pair to a U11-A27 base pair. The nearest-neighbor model in the stems predicts  $\Delta G_{37, \text{PSK-4A-U11A27}}^0 - \Delta G_{37, \text{PSK-4A}}^0$  to be 1.4 kcal/mol, and the SPM predicts  $\Delta G_{37, \text{PSK-4A-U11A27}}^0 - \Delta G_{37, \text{PSK-U11A27}}^0$  to be ~1.0 kcal/mol. The FCA experiments for mutation from PSK-4A and PSK-U11A27 to PSK-4A-U11A27 give  $\Delta\Delta G_{37}^0$  values of -1.1 and -1.2 kcal/mol, respectively. This is surprising because the mutations make the pseudoknot more stable rather than less stable as expected. The deviation could come from additional tertiary interactions between one or more A's in loop 1 and the UA pair in stem 2. For example, an A·A-U base triple with the non-Watson-Crick A in the major groove is possible (78, 79). Another new interaction perhaps facilitated by the increased flexibility of an A-U compared to a G-C pair is also possible. That suggests again that stem-loop tertiary interactions can be a large factor for the free energy of a pseudoknot.

**Model for Pseudoknot Free Energy Estimation.** The sequence dependence of stabilities for modified BWYV pseudoknots provides insight into several factors important for predictions. (1) The INN-HB model can be used to estimate the free energy contribution from stem 2 if tertiary interactions are not involved. Because the crystal structure of the BWYV pseudoknot indicates that stem 2 has a propeller twist that deviates more from A-form than stem 1, this suggests that the INN-HB model will also work the same way for stem 1. (2) As reported previously (44, 75), tertiary interactions between the stem and loop are a major contributor to pseudoknot free energy. For example, a possible newly formed A·A-U base triple in the stem 2–loop 1 region in PSK-4A-U11A27 could stabilize the pseudoknot by -2.2 kcal/mol. In the BWYV pseudoknot, the structure in the joint part of the stem 1–loop 3 region and stem 2–loop 1 region is “distorted” and an expected base pair with coaxial stacking in the secondary structure is therefore absent. The free energy loss for this distortion, however, can be compensated by the tertiary interactions (Figure 1C). Thus, in the absence of structural information and thermodynamic parameters for tertiary interactions, it is reasonable to include possible base pairs and coaxial stacking at the joint in predicting the free energy of a pseudoknot. These interactions are possible, so their absence implies that the tertiary interactions must be even more favorable. (3) The statistical polymer model (SPM) provides excellent approximations for the length dependence of loop 1. There will also be sequence dependence, however, which is not dependent on tertiary interactions. For example, oligo-C loops are unusually unstable.

The following model for predicting pseudoknot stability is consistent with FCA results:

$$\begin{aligned}\Delta G_{\text{PSK}}^0 = & \sum \Delta G_{\text{stems}}^0 - T \sum S_{\text{loops}}^0 + \Delta G_{\text{assemble}}^0 \\ & + \Delta G_{\text{coaxial stacking}}^0 + \Delta G_{\text{loop sequence}}^0 + \Delta G_{\text{net of tertiaries}}^0\end{aligned}\quad (23)$$

As in SPM (42),  $\Delta G_{\text{stems}}^0$  and possible  $\Delta G_{\text{coaxial stacking}}^0$  can be calculated with nearest-neighbor parameters (39, 63), and  $S_{\text{loops}}^0$  and  $\Delta G_{\text{assemble}}^0$  can be calculated from statistical mechanics using a lattice model (42).  $\Delta G_{\text{loop sequence}}^0$  is a term that will require many more experiments before approximations are available beyond oligo-C penalties. The  $\Delta G_{\text{net of tertiaries}}^0$  term accounts for tertiary interactions between the stems and loops, and there is currently no good model for calculating it. Presumably, the three-dimensional structure of the pseudoknot is important for allowing nucleotides to interact, and certain base triples will be especially stable. Further experiments and comparisons with and between structures are needed to provide approximations, but the inclusion of possible base pairs and coaxial stacking at the interface limits the underestimation of pseudoknot stability due to the lack of approximations for  $\Delta G_{\text{net of tertiaries}}^0$ .

## CONCLUSION

Fluorescence competition assays (FCA) based on FRET or quenching of fluorescence by nucleotides provide thermodynamic information about pseudoknots. The method has an advantage in that it probes a certain transition at a defined temperature and does not require a temperature extrapolation. The method is sensitive and therefore requires small amounts of sample. This allowed measurements of the sequence dependence of stability contributions from elements in the loop 1–stem 2 region of pseudoknots. In general, fluorescence competition assays allow systematic studies of RNA stability that can inform writing of algorithms for predicting and/or designing RNA secondary structures.

In agreement with previous studies (44, 75), tertiary interactions can provide large contributions to pseudoknot free energy that can be on the same order of magnitude as those from a Watson-Crick base pair. The free energy from the loops can be estimated with the statistical polymer model of Cao and Chen (42), which will eventually require augmentation with a sequence-dependent term. This is similar to approaches in algorithms for predicting RNA secondary structure, where a length-dependent increment for loops is augmented with a sequence-dependent increment (60). Further experiments are necessary for understanding the sequence dependence of thermodynamics for the stem 1–loop 3 region and for tertiary interactions. In the absence of in-depth knowledge of the sequence dependence of stability, however, rapidly acquired experimental constraints from NMR spectra can be used to reveal pseudoknot structures (38).

## ACKNOWLEDGMENT

We thank Dan Wang for fitting titration curves with SAS, Dr. Gang Chen for comments on the manuscript, and Prof. David Mathews for suggesting fluorescence competition assays.

## SUPPORTING INFORMATION AVAILABLE

(I) Calculation of the free energies for formation of pseudoknots from unfolded RNA by models in NUPACK and SPM

and free energies for formation of stem 1 hairpins and the reference structures from unfolded RNA. (II) Calculation of  $\Delta G_{37,437D}^0$  PSK from  $\Delta G_{37,BWYV}^0$  PSK 1 and  $\Delta G_{37,BWYV}^0$  PSK 2. (III) Plots of published  $\Delta H^0$  values vs  $T_m$  for BWYV. This material is available free of charge via the Internet at <http://pubs.acs.org>.

## REFERENCES

- Rietveld, K., Van Poelgeest, R., Pleij, C. W., Van Boom, J. H., and Bosch, L. (1982) The tRNA-like structure at the 3' terminus of turnip yellow mosaic virus RNA: Differences and similarities with canonical tRNA. *Nucleic Acids Res.* 10, 1929–1946.
- Brierley, I., Pennell, S., and Gilbert, R. J. C. (2007) Viral RNA pseudoknots: Versatile motifs in gene expression and replication. *Nat. Rev. Microbiol.* 5, 598–610.
- Egli, M., Minasov, G., Su, L., and Rich, A. (2002) Metal ions and flexibility in a viral RNA pseudoknot at atomic resolution. *Proc. Natl. Acad. Sci. U.S.A.* 99, 4302–4307.
- Brink, M. F., Verbeet, M. P., and de Boer, H. A. (1993) Formation of the central pseudoknot in 16S rRNA is essential for initiation of translation. *EMBO J.* 12, 3987–3996.
- Juzumiene, D. I., and Wollenzien, P. (2001) Arrangement of the central pseudoknot region of 16S rRNA in the 30S ribosomal subunit determined by site-directed 4-thiouridine crosslinking. *RNA* 7, 71–84.
- McPheeeters, D. S., Stormo, G. D., and Gold, L. (1988) Autogenous regulatory site on the bacteriophage T4 gene 32 messenger RNA. *J. Mol. Biol.* 201, 517–535.
- Tang, C. K., and Draper, D. E. (1989) Unusual mRNA pseudoknot structure is recognized by a protein translational repressor. *Cell* 57, 531–536.
- Du, Z. H., and Hoffman, D. W. (1997) An NMR and mutational study of the pseudoknot within the gene 32 mRNA of bacteriophage T2: Insights into a family of structurally related RNA pseudoknots. *Nucleic Acids Res.* 25, 1130–1135.
- Cornish, P. V., Stammmer, S. N., and Giedroc, D. P. (2006) The global structures of a wild-type and poorly functional plant luteoviral mRNA pseudoknot are essentially identical. *RNA* 12, 1959–1969.
- Kierzek, E., Christensen, S. M., Eickbush, T. H., Kierzek, R., Turner, D. H., and Moss, W. N. (2009) Secondary structures for 5' regions of R2 retrotransposon RNAs reveal a novel conserved pseudoknot and regions that evolve under different constraints. *J. Mol. Biol.* 390, 428–442.
- Nonin-Lecomte, S., Felden, B., and Dardel, F. (2006) NMR structure of the *Aquifex aeolicus* tmRNA pseudoknot PK1: New insights into the recoding event of the ribosomal trans-translation. *Nucleic Acids Res.* 34, 1847–1853.
- Nameki, N., Felden, B., Atkins, J. F., Gesteland, R. F., Himeno, H., and Muto, A. (1999) Functional and structural analysis of a pseudoknot upstream of the tag-encoded sequence in *E. coli* tmRNA. *J. Mol. Biol.* 286, 733–744.
- Soukup, G. A. (2006) Core requirements for glmS ribozyme self-cleavage reveal a putative pseudoknot structure. *Nucleic Acids Res.* 34, 968–975.
- Jeng, K. S., Daniel, A., and Lai, M. M. C. (1996) A pseudoknot ribozyme structure is active in vivo and required for hepatitis delta virus RNA replication. *J. Virol.* 70, 2403–2410.
- Chen, G., Wen, J. D., and Tinoco, I. (2007) Single-molecule mechanical unfolding and folding of a pseudoknot in human telomerase RNA. *RNA* 13, 2175–2188.
- ten Dam, E., van Belkum, A., and Pleij, K. (1991) A conserved pseudoknot in telomerase RNA. *Nucleic Acids Res.* 19, 6951–6951.
- Qiao, F., and Cech, T. R. (2008) Triple-helix structure in telomerase RNA contributes to catalysis. *Nat. Struct. Mol. Biol.* 15, 634–640.
- Comolli, L. R., Smirnov, I., Xu, L., Blackburn, E. H., and James, T. L. (2002) A molecular switch underlies a human telomerase disease. *Proc. Natl. Acad. Sci. U.S.A.* 99, 16998–17003.
- Held, D. M., Kissel, J. D., Thacker, S. J., Michalowski, D., Saran, D., Ji, J. F., Hardy, R. W., Rossi, J. J., and Burke, D. H. (2007) Cross-clade inhibition of recombinant human immunodeficiency virus type 1 (HIV-1), HIV-2, and simian immunodeficiency virus SIVcpz reverse transcriptases by RNA pseudoknot aptamers. *J. Virol.* 81, 5375–5384.
- Namy, O., Moran, S. J., Stuart, D. I., Gilbert, R. J. C., and Brierley, I. (2006) A mechanical explanation of RNA pseudoknot function in programmed ribosomal frameshifting. *Nature* 441, 244–247.
- Brierley, I., Digard, P., and Inglis, S. C. (1989) Characterization of an efficient coronavirus ribosomal frameshifting signal: Requirement for an RNA pseudoknot. *Cell* 57, 537–547.
- Heppell, B., and Lafontaine, D. A. (2008) Folding of the SAM aptamer is determined by the formation of a K-turn-dependent pseudoknot. *Biochemistry* 47, 1490–1499.
- Atkins, J. F., Gesteland, R. F., Jackson, R. J., and Wills, N. M. (2006) The shapely mRNA: Knotting ventured, knotting gained. In *The RNA World* (Gesteland, R. F., Cech, T. R., and Atkins, J. F., Eds.) 3rd ed., Cold Spring Harbor Laboratory Press, Plainview, NY.
- Wyatt, J. R., Puglisi, J. D., and Tinoco, I. Jr. (1990) RNA pseudoknots: Stability and loop size requirements. *J. Mol. Biol.* 214, 455–470.
- van Batenburg, F. H., Gulyaev, A. P., Pleij, C. W., Ng, J., and Oliehoek, J. (2000) PseudoBase: A database with RNA pseudoknots. *Nucleic Acids Res.* 28, 201–204.
- Aalberts, D. P., and Hodas, N. O. (2005) Asymmetry in RNA pseudoknots: Observation and theory. *Nucleic Acids Res.* 33, 2210–2214.
- Kang, H. S., and Tinoco, I. Jr. (1997) A mutant RNA pseudoknot that promotes ribosomal frameshifting in mouse mammary tumor virus. *Nucleic Acids Res.* 25, 1943–1949.
- Chen, X., Chamorro, M., Lee, S. I., Shen, L. X., Hines, J. V., Tinoco, I. Jr., and Varma, H. E. (1995) Structural and functional studies of retroviral RNA pseudoknots involved in ribosomal frameshifting: Nucleotides at the junction of the two stems are important for efficient ribosomal frameshifting. *EMBO J.* 14, 842–852.
- Chen, J. L., Blasco, M. A., and Greider, C. W. (2000) Secondary structure of vertebrate telomerase RNA. *Cell* 100, 503–514.
- Theimer, C. A., Finger, L. D., Trantirek, L., and Feigon, J. (2003) Mutations linked to dyskeratosis congenita cause changes in the structural equilibrium in telomerase RNA. *Proc. Natl. Acad. Sci. U.S.A.* 100, 449–454.
- Gulyaev, A. P., Heus, H. A., and Olsthoorn, R. C. (2007) An RNA conformational shift in recent H5N1 influenza A viruses. *Bioinformatics* 23, 272–276.
- Rivas, E., and Eddy, S. R. (1999) A dynamic programming algorithm for RNA structure prediction including pseudoknots. *J. Mol. Biol.* 285, 2053–2068.
- Dirks, R. M., and Pierce, N. A. (2003) A partition function algorithm for nucleic acid secondary structure including pseudoknots. *J. Comput. Chem.* 24, 1664–1677.
- Ren, J., Rastegari, B., Condon, A., and Hoos, H. H. (2005) HotKnots: Heuristic prediction of RNA secondary structures including pseudoknots. *RNA* 11, 1494–1504.
- Gulyaev, A. P., van Batenburg, F. H., and Pleij, C. W. (1995) The computer simulation of RNA folding pathways using a genetic algorithm. *J. Mol. Biol.* 250, 37–51.
- Abrahams, J. P., van den Berg, M., van Batenburg, E., and Pleij, C. (1990) Prediction of RNA secondary structure, including pseudoknotting, by computer simulation. *Nucleic Acids Res.* 18, 3035–3044.
- Xayaphoummine, A., Bucher, T., and Isambert, H. (2005) Kinfold web server for RNA/DNA folding path and structure prediction including pseudoknots and knots. *Nucleic Acids Res.* 33, W605–W610.
- Hart, J. M., Kennedy, S. D., Mathews, D. H., and Turner, D. H. (2008) NMR-assisted prediction of RNA secondary structure: Identification of a probable pseudoknot in the coding region of an R2 retrotransposon. *J. Am. Chem. Soc.* 130, 10233–10239.
- Xia, T., SantaLucia, J. Jr., Burkard, M. E., Kierzek, R., Schroeder, S. J., Jiao, X., Cox, C., and Turner, D. H. (1998) Thermodynamic parameters for an expanded nearest-neighbor model for formation of RNA duplexes with Watson-Crick base pairs. *Biochemistry* 37, 14719–14735.
- SantaLucia, J. Jr., and Turner, D. H. (1997) Measuring the thermodynamics of RNA secondary structure formation. *Biopolymers* 44, 309–319.
- Gulyaev, A. P., van Batenburg, F. H., and Pleij, C. W. (1999) An approximation of loop free energy values of RNA H-pseudoknots. *RNA* 5, 609–617.
- Cao, S., and Chen, S. J. (2006) Predicting RNA pseudoknot folding thermodynamics. *Nucleic Acids Res.* 34, 2634–2652.
- Theimer, C. A., and Giedroc, D. P. (1999) Equilibrium unfolding pathway of an H-type RNA pseudoknot which promotes programmed –1 ribosomal frameshifting. *J. Mol. Biol.* 289, 1283–1299.
- Nixon, P. L., and Giedroc, D. P. (2000) Energetics of a strongly pH dependent RNA tertiary structure in a frameshifting pseudoknot. *J. Mol. Biol.* 296, 659–671.
- Soto, A. M., Misra, V., and Draper, D. E. (2007) Tertiary structure of an RNA pseudoknot is stabilized by “diffuse”  $Mg^{2+}$  ions. *Biochemistry* 46, 2973–2983.
- Theimer, C. A., and Giedroc, D. P. (2000) Contribution of the intercalated adenosine at the helical junction to the stability of the

- gag-pro frameshifting pseudoknot from mouse mammary tumor virus. *RNA* 6, 409–421.
47. Theimer, C. A., Wang, Y., Hoffman, D. W., Krisch, H. M., and Giedroc, D. P. (1998) Non-nearest neighbor effects on the thermodynamics of unfolding of a model mRNA pseudoknot. *J. Mol. Biol.* 279, 545–564.
  48. Nixon, P. L., and Giedroc, D. P. (1998) Equilibrium unfolding (folding) pathway of a model H-type pseudoknotted RNA: The role of magnesium ions in stability. *Biochemistry* 37, 16116–16129.
  49. Qiu, H., Kaluarachchi, K., Du, Z., Hoffman, D. W., and Giedroc, D. P. (1996) Thermodynamics of folding of the RNA pseudoknot of the T4 gene 32 autoregulatory messenger RNA. *Biochemistry* 35, 4176–4186.
  50. Vander Meulen, K. A., Davis, J. H., Foster, T. R., Record, M. T., Jr., and Butcher, S. E. (2008) Thermodynamics and folding pathway of tetraloop receptor-mediated RNA helical packing. *J. Mol. Biol.* 384, 702–717.
  51. Harrison, J. G., Liu, X., and Balasubramanian, S. (1999) Screening for oligonucleotide binding affinity by a convenient fluorescence competition assay. *Nucleic Acids Res.* 27, e14.
  52. Hopkins, J. F., and Woodson, S. A. (2005) Molecular beacons as probes of RNA unfolding under native conditions. *Nucleic Acids Res.* 33, 5763–5770.
  53. Gelfand, C. A., Plum, G. E., Mielewczik, S., Remeta, D. P., and Breslauer, K. J. (1999) A quantitative method for evaluating the stabilities of nucleic acids. *Proc. Natl. Acad. Sci. U.S.A.* 96, 6113–6118.
  54. Kim, Y. C., Su, L., Maas, S., O'Neill, A., and Rich, A. (1999) Specific mutations in a viral RNA pseudoknot drastically change ribosomal frameshifting efficiency. *Proc. Natl. Acad. Sci. U.S.A.* 96, 14234–14239.
  55. Su, L., Chen, L., Egli, M., Berger, J. M., and Rich, A. (1999) Minor groove RNA triplex in the crystal structure of a ribosomal frameshifting viral pseudoknot. *Nat. Struct. Biol.* 6, 285–292.
  56. Borer, P. N. (1975) Optical properties of nucleic acids, absorption and circular dichroism spectra. In *Handbook of Biochemistry and Molecular Biology: Nucleic Acids* (Fasman, G. D., Ed.) 3rd ed., pp 589–595, CRC Press, Cleveland, OH.
  57. Richards, E. G. (1975) Use of tables in calculation of absorption, optical rotatory dispersion and circular dichroism of polyribonucleotides. In *Handbook of Biochemistry and Molecular Biology: Nucleic Acids* (Fasman, G. D., Ed.) 3rd ed., pp 596–603, CRC Press, Cleveland, OH.
  58. Petersheim, M., and Turner, D. H. (1983) Base-stacking and base-pairing contributions to helix stability: Thermodynamics of double-helix formation with CCGG, CCGGp, CCGGAp, ACCGGp, CCGGU<sub>p</sub>, and ACCGGU<sub>p</sub>. *Biochemistry* 22, 256–263.
  59. McDowell, J. A., and Turner, D. H. (1996) Investigation of the structural basis for thermodynamic stabilities of tandem GU mismatches: solution structure of (rGAGGUCUC)<sub>2</sub> by two-dimensional NMR and simulated annealing. *Biochemistry* 35, 14077–14089.
  60. Mathews, D. H., Disney, M. D., Childs, J. L., Schroeder, S. J., Zuker, M., and Turner, D. H. (2004) Incorporating chemical modification constraints into a dynamic programming algorithm for prediction of RNA secondary structure. *Proc. Natl. Acad. Sci. U.S.A.* 101, 7287–7292.
  61. O'Toole, A. S., Miller, S., Haines, N., Zink, M. C., and Serra, M. J. (2006) Comprehensive thermodynamic analysis of 3' double-nucleotide overhangs neighboring Watson-Crick terminal base pairs. *Nucleic Acids Res.* 34, 3338–3344.
  62. Clanton-Arrowood, K., McGurk, J., and Schroeder, S. J. (2008) 3' terminal nucleotides determine thermodynamic stabilities of mismatches at the ends of RNA helices. *Biochemistry* 47, 13418–13427.
  63. Walter, A. E., and Turner, D. H. (1994) Sequence dependence of stability for coaxial stacking of RNA helices with Watson-Crick base paired interfaces. *Biochemistry* 33, 12715–12719.
  64. Turner, D. H. (2000) Conformational Changes. In *Nucleic Acids: Structures, properties, and functions* (Bloomfield, V. A., Crothers, D. M., and Tinoco, I., Eds.) pp 259–334, University Science Books, Sausalito, CA.
  65. Mathews, D. H., and Turner, D. H. (2006) Prediction of RNA secondary structure by free energy minimization. *Curr. Opin. Struct. Biol.* 16, 270–278.
  66. Milligan, J. F., Groebe, D. R., Witherell, G. W., and Uhlenbeck, O. C. (1987) Oligoribonucleotide synthesis using T7 RNA polymerase and synthetic DNA templates. *Nucleic Acids Res.* 15, 8783–8798.
  67. Shiman, R., and Draper, D. E. (2000) Stabilization of RNA tertiary structure by monovalent cations. *J. Mol. Biol.* 302, 79–91.
  68. Vieregg, J., Cheng, W., Bustamante, C., and Tinoco, I., Jr. (2007) Measurement of the effect of monovalent cations on RNA hairpin stability. *J. Am. Chem. Soc.* 129, 14966–14973.
  69. Nakano, S., Fujimoto, M., Hara, H., and Sugimoto, N. (1999) Nucleic acid duplex stability: Influence of base composition on cation effects. *Nucleic Acids Res.* 27, 2957–2965.
  70. Mikulecky, P. J., and Feig, A. L. (2006) Heat capacity changes associated with nucleic acid folding. *Biopolymers* 82, 38–58.
  71. Lu, Z. J., Turner, D. H., and Mathews, D. H. (2006) A set of nearest neighbor parameters for predicting the enthalpy change of RNA secondary structure formation. *Nucleic Acids Res.* 34, 4912–4924.
  72. Laing, L. G., and Hall, K. B. (1996) A model of the iron responsive element RNA hairpin loop structure determined from NMR and thermodynamic data. *Biochemistry* 35, 13586–13596.
  73. Dale, T., Smith, R., and Serra, M. J. (2000) A test of the model to predict unusually stable RNA hairpin loop stability. *RNA* 6, 608–615.
  74. Bloomfield, V. A., Crothers, D. M., and Tinoco, I., Jr. (2000) Nucleic Acid Structures from Diffraction Methods. In *Nucleic Acids: Structures, properties, and functions*, p 100, University Science Books, Sausalito, CA.
  75. Nixon, P. L., Cornish, P. V., Suram, S. V., and Giedroc, D. P. (2002) Thermodynamic analysis of conserved loop-stem interactions in P1-P2 frameshifting RNA pseudoknots from plant Luteoviridae. *Biochemistry* 41, 10665–10674.
  76. Groebe, D. R., and Uhlenbeck, O. C. (1988) Characterization of RNA hairpin loop stability. *Nucleic Acids Res.* 16, 11725–11735.
  77. Freier, S. M., Hill, K. O., Dewey, T. G., Marky, L. A., Breslauer, K. J., and Turner, D. H. (1981) Solvent effects on the kinetics and thermodynamics of stacking in poly(cytidyllic acid). *Biochemistry* 20, 1419–1426.
  78. Ban, N., Nissen, P., Hansen, J., Moore, P. B., and Steitz, T. A. (2000) The complete atomic structure of the large ribosomal subunit at 2.4 angstrom resolution. *Science* 289, 905–920.
  79. Nagaswamy, U., Larios-Sanz, M., Hurley, J., Collins, S., Zhang, Z. D., Zhao, Q., and Fox, G. E. (2002) NCIR: A database of non-canonical interactions in known RNA structures. *Nucleic Acids Res.* 30, 395–397.